Thermoelectric properties of new Bi-chalcogenide layered compounds

Yoshikazu Mizuguchi, Atsuhiro Nishida, Atsushi Omachi, and Osuke Miura

Tokyo Metropolitan University, 1-1, Minami-osawa, Hachioji 192-0397, Japan.

Abstract

The layered Bi-chalcogenide compounds have been drawing much attention as a new layered superconductor family since 2012. Due to the rich variation of crystal structure and constituent elements, the development of new physics and chemistry of the layered Bi-chalcogenide family and its applications as functional materials have been expected. Recently, it was revealed that the layered Bi chalcogenides can show a relatively high thermoelectric performance (ZT = 0.36 in LaOBiSSe at ~650 K). Here, we show the crystal structure variation of the Bi-chalcogenide family and their thermoelectric properties. Finally, the possible strategies for enhancing the thermoelectric performance are discussed on the basis of the experimental and the theoretical facts reviewed here.

1. Introduction

Thermoelectric energy conversion is a promising technology for solving energy problems because the energy of the waste heat can be directly converted to the electrical energy. So far, the available thermoelectric devises have been limited due to the absence of high performance thermoelectric materials. To estimate the performance of thermoelectric materials, dimensionless figure-of-merit (ZT) is generally used. The ZT can be calculated as $ZT = S^2T/\rho\kappa$, where S, T, ρ, and κ are Seebeck coefficient, absolute temperature, electrical resistivity, and thermal conductivity, respectively. Hence, a large absolute value of the Seebeck coefficient, low electrical resistivity, and low thermal conductivity are required for a high ZT. Typically, in a conventional semiconductor, S is proportional to T/n, where n is carrier concentration with a single band approximation. The ρ is proportional to $1/en\mu$, where μ is carrier mobility. Therefore, insulators (or semiconductors with a large band gap) exhibit large absolute S, but their ρ is usually large. In contrast, metallic compounds exhibit low ρ, but absolute S of metallic compounds is generally small. Due to this trade-off relationship of the electrical factors (S and ρ), the enhancement of S^2/ρ (power factor: PF) is quite difficult. The material, which satisfies both large S and low ρ, is semiconductors with a narrow band gap [1]. For example, the Bi_2Te_3 family possesses such a band structure and shows a high performance of $ZT \sim 1$ at around 300 K due to the large μ and the suitable n [2,3]. Hence, Bi_2Te_3-based compounds have been used as a practical thermoelectric material for a long time [2]. Another strategy for enhancing ZT is the use of the quantum-size effect. The ZT of Bi_2Te_3-based system can be enhanced up to 2.4 by fabricating the Bi_2Te_3/Sb_2Te_3 super-lattice devise [4,5]. In addition, the quantum-size effect can be expected to positively work in enhancing ZT in the compounds with a *layered structure*. One of the examples is the layered Co oxides, such as $NaCoO_2$ and related layered compounds [6-8]. These compounds show anomalously large S owing to the strong electron correlations, and the κ of these compounds is reduced by the phonon scattering at the interface of the layers. In addition, layered compounds typically possess the great flexibilities of stacking structure and constituent elements as demonstrated in the Co oxides [6-8], which results in the desirable tuning of the electronic structure and the local crystal structure. Therefore, one can say that the layered structure is greatly suitable for designing high ZT materials.

In 2012, we discovered new layered superconductors whose crystal structure is composed of the alternate stacks of the BiS_2 bilayer (electrically *conducting layer*) and the electrically insulating *blocking layers* [9-11]. The parent phase (for example, $LaOBiS_2$ with the structure of Fig. 1(a)) is a semiconductor with a band gap [9,12]. When electron carriers were generated in the Bi-6p orbitals by partial substitutions of O by F (in the La_2O_2 blocking layers), the F-substituted compounds ($LaO_{1-x}F_xBiS_2$) becomes metallic and shows superconductivity at low temperatures [10,12]. Furthermore, the La_2O_2 blocking layer can be replaced by the RE_2O_2 layers (RE: rare earth or Bi) or other oxide (or fluoride) layers as shown in Fig. 1. Indeed, the crystal structure can be

flexibly modified by changing the blocking layer structure in the BiS_2-based compound family [11]. Focusing on the electronic state, we noted that the calculated bad gap were relatively small, and some parent compounds showed low electrical resistivity (as compared normal semiconductors). In addition, the thermal conductivity of the $LaO_{1-x}F_xBiS_2$ samples were relatively small [13]. Thus, we considered that the BiS_2-based layered compounds could be a layered thermoelectric material family as the Bi-Te family or the layered Co oxides family. In this article, the crystal structure variation of the layered Bi-chalcogenide family and the physical properties of those Bi chalcogenides are reviewed. Finally, the possible strategies for enhancing thermoelectric properties of the Bi chalcogenides are discussed.

This article contains new (unpublished) results on $CeO_{1-x}F_xBiS_2$, $NdO_{1-x}F_xBiS_2$, and $LaOBiPbS_3$. Therefore, we briefly explain the experimental procedures. The polycrystalline samples were prepared using a conventional solid-state-reaction method with reaction temperatures of 700-800 ℃. The purity and the crystal structure of the obtained samples were investigated using powder X-ray diffraction. The reaction or the annealing processes were carried out in an evacuated quartz tube. Temperature dependence of ρ and S were measured using a four-terminal method with ZEM-3 (Advance Riko).

2. Crystal structure of layered Bi chalcogenides

Typical crystal structures of the layered Bi chalcogenides are summarized in Fig. 1. All the compounds have a layered structure composed of the alternate stacks of the electrically conducting layer and the electrically insulating blocking layer. The typical structures are categorized into the tetragonal (*P*4/*nmm* or *I*4/*mmm*) space group. These Bi chalcogenides have NaCl-type Bi-Ch conducting layers: Bi_2Ch_4 layer ($BiCh_2$ bilayer) or M_4Ch_6 layer (M: Bi, Pb). Since the conducting layers contain a two-dimensional Bi-Ch square lattice, the layered Bi chalcogenides exhibit two-dimensional electrical transport.

Figures 1(a-c) are the crystal structures of BiS_2-based compounds with the BiS_2 bilayer (Bi_2S_4 layer) as a conducting layer. Among them, the $REOBiCh_2$ (RE: rare earth or Bi; Ch: S or Se) structure (Fig. 1(a)) is the most popular one. In this structure, the Bi_2S_4 layer is a conducting layer, and the RE_2O_2 layer acts as a blocking layer. When electron carriers were doped by partial substitutions of O by F, the $RE(O,F)BiCh_2$ compounds become a superconductor with a superconducting transition temperature (T_c) as high as 11 K [10,11]. The RE site of $RE(O,F)BiS_2$ can be occupied by La, Ce, Pr, Nd, Sm, Yb, and Bi [10,14-22]. In the case of RE = La, the RE site can be partially substituted with Y, Ti, Zr, Hf, and Th [23,24]. In addition, the S site can be substituted by Se. The $RE(O,F)BiS_{2-x}Se_x$-type compounds were reported for RE = La, Ce, and Nd [25-29]. Furthermore, the end member $La(O,F)BiSe_2$ can be synthesized for RE = La [30].

The RE$_2$O$_2$ layer of the REOBiS$_2$ structure can be replaced with the Sr$_2$F$_2$ or Eu$_2$F$_2$ layer, which results in the SrFBiS$_2$ or EuFBiS$_2$ compound [31,32]. The Sr (or Eu) site can be partially substituted by RE; the RE substitution dopes electron carriers into the BiS$_2$ layer [34,35]. In addition, the Sr site can be partially substituted by Ca [32]. Owing to these great flexibility on element substitutions for the RE and Ch sites, the REOBiCh$_2$-type structure has been actively studied, and is particularly important to understand the physical properties of the layered Bi-chalcogenide family.

Figure 1(b) is a crystal structure of Eu$_3$F$_4$Bi$_2$S$_4$ [36] with a Eu$_3$F$_4$ blocking layer. The Eu$_3$F$_4$ layer can be regarded as the double Eu$_2$F$_2$ layers combined to each other with Eu-site sharing. The material itself is a superconductor, and the superconducting T_c was enhanced by Se substitution in Eu$_3$F$_4$Bi$_2$S$_{2-x}$Se$_x$ [37].

Figure 1(c) is a crystal structure of Bi$_4$O$_4$SO$_4$Bi$_2$S$_4$, whose structure can be regarded as the alternate stacks of the Bi$_4$O$_4$SO$_4$ blocking layer and the Bi$_2$S$_4$ conducting layer (BiS$_2$ bilayer). It has been considered that the SO$_4$ site in the blocking layer can have some defects, which provides electron carriers into the BiS$_2$ layers [9]. Indeed, the Bi$_4$O$_4$S$_3$ compound with 50% SO$_4$ defects (namely, Bi$_4$O$_4$(SO$_4$)$_{0.5}$Bi$_2$S$_4$) becomes a superconductor with $T_c \sim 5$ K [9]. Due to the difficulty in determining the SO$_4$ site structure using polycrystalline samples and the absence of single crystals, the precise determination of the SO$_4$ site structure (and the composition) has not been achieved yet [38]; some reports suggested the Bi$_3$O$_2$S$_3$ (= Bi$_4$O$_4$S$_2$Bi$_2$S$_4$) phase was also formed and showed superconductivity [39,40].

Recently, a new Bi-chalcogenide compound with a thick conducting layer of M$_4$S$_6$ (M = Bi, Pb) was synthesized. Figure 1(d) shows the crystal structure of LaOBiPbS$_3$ [41]. In this structure, an NaCl-type M-S block (layer) is intercalated at between BiS$_2$ layers. Also, this conducting layer can be regarded as the 4-layer-type structure. Thus, the crystal structure variation can be developed by fabricating the multi-layer-type conducting layers as well as by changing the blocking layer structure as demonstrated in the structures of Fig. 1(a-c). We note that the distorted-NaCl-type M$_4$S$_6$ conducting layer is structurally similar to the Bi$_4$Te$_6$ conducting layer of CsBi$_4$Te$_6$, which is a known thermoelectric material (Fig. 1(e)) [3], although the space group of CsBi$_4$Te$_6$ (monoclinic $C2/m$) is different from that of LaOBiPbS$_3$ and the BiS$_2$-based compounds (tetragonal $P4/nmm$ or $I4/mmm$). The structural symmetry lowering from tetragonal to monoclinic was recently revealed in a single crystal of LaOBiS$_2$ by synchrotron X-ray experiments [42]. Although the X-ray diffraction (XRD) with the polycrystalline LaOBiS$_2$ samples suggested the space group of tetragonal $P4/nmm$, the crystal structure of the LaOBiS$_2$ single crystal was determined to be monoclinic $P2_1/m$. This different results in between polycrystalline and single crystal samples would indicate the crystal structure instability in the BiS$_2$-based compounds. At the same time, the structure instability can be regarded as the *structure flexibility* in the same group of compounds. Thus, we consider that the Bi-chalcogenide family possesses great flexibility of crystal structure (including space group,

stacking sequence, and constituent elements), and hence, it is very useful to explore new materials with a high thermoelectric performance.

3. Thermoelectric properties of LaOBiS$_2$-based compounds

3-1. LaO$_{1-x}$F$_x$BiS$_2$

Here, we focus on the LaOBiS$_2$ systems. As introduced above, LaOBiS$_2$ is one of the parent phases of the BiS$_2$-based superconductor, and shows semiconducting-like electrical transport below the room temperature [10]. Band calculations suggested that the LaOBiS$_2$ is a semiconductor with a relatively narrow band gap ($<$ 1 eV) [12]. Partial substitutions of the O site by F generate electron carriers in the BiS$_2$ conducting layers, and the F-substituted LaO$_{1-x}$F$_x$BiS$_2$ shows a superconducting transition at low temperatures [10]. We considered the LaOBiS$_2$-based compounds could exhibit a high thermoelectric properties since we observed a low thermal conductivity in the LaO$_{1-x}$F$_x$BiS$_2$ samples (κ ~ 2 W/mK at 300 K) [13]. Thus, we measured high-temperature thermoelectric properties (ρ, S, and PF) of LaO$_{1-x}$F$_x$BiS$_2$ and investigated the effect of the F substitution (electron doping) to the thermoelectric properties [43].

Figures 2(a-c) show the temperature dependences of (a) ρ, (b) S, and (c) PF for LaO$_{1-x}$F$_x$BiS$_2$. As depicted in Fig. 1(d), the electron carrier concentration is expected to increase with increasing F concentration. The ρ of $x = 0$ increases with increasing temperature, and an anomaly (a hump) is observed at around 500 K. Although the origin of the anomaly has not been clarified yet, it may be related to the (local) structure distortion because the crystal structure of LaOBiS$_2$ can be distorted into monoclinic as revealed in the single crystal structure analysis using synchrotron X-ray [42]. With increasing F concentration, the values of ρ decrease at whole temperatures. The S was negative for all the F concentration at whole temperatures (tested in these experiments), which indicates that the mainly-contributing carrier is electron in this system. The absolute value of S increases with increasing temperature. One of the important facts is the absolute S largely decreases with increasing F concentration. As a result, the values of the PF rapidly decrease with F substitution as shown in Fig. 2(c). Indeed, in the LaOBiS$_2$ system, the electron doping obviously degrades the thermoelectric properties [13,43]. To enhance the thermoelectric performance (PF) in the LaOBiS$_2$ system, decreasing ρ without degradation of the absolute S is required. Thus, we next investigated the effects of partial substitutions of S by Se in the conducting layers.

3-2. LaOBiS$_{2-x}$Se$_x$

The S site of LaOBiS$_2$ can be partially substituted by Se [44]. In LaOBiS$_{2-x}$Se$_x$, both S and Se have the same valence of -2 (S^{2-} and Se^{2-}). Hence, the Se substitution does not affect the valence of Bi and does not dope electrons, but it should affect the band structure because of the difference of

5

ionic radii of S^{2-} (184 pm) and Se^{2-} (198 pm). Upon the substitution of larger Se^{2-}, the enhancement of the orbital overlap between Bi and Ch should be expected.

Figures 3(a-c) show the temperature dependences of (a) ρ, (b) S, and (c) PF for LaOBiS$_{2-x}$Se$_x$ [44]. Figure 3(d) is the crystal structure of LaOBiS$_{2-x}$Se$_x$ and the definitions of the Ch1 and the Ch2 sites. With increasing Se concentration, the values of ρ decrease, indicating that the Se substitution enhances electric conductivity in LaOBiS$_{2-x}$Se$_x$. The values of S are all negative as observed in LaO$_{1-x}$F$_x$BiS$_2$, which suggests that the electrons are mainly contributing in electrical transport in LaOBiS$_{2-x}$Se$_x$. The absolute values of S do not show a remarkable change up to $x = 0.6$, and it slightly decreases at $x = 0.8$ and 1. The small changes in the S with increasing Se concentration imply that the carrier concentration is not largely affected by the Se substitution. In addition, as will be shown later, the densified LaOBiSSe sample shows the S value comparable to that of LaOBiS$_2$. Thus, we consider that the Se substitution does not largely affect carrier concentration, but it enhances metallic conductivity due to the enhanced carrier mobility; actually, the large enhancement of mobility with increasing Se concentration was revealed in our recent Hall measurements [45]. This can be understood with the concept of in-plane chemical pressure effect as demonstrated in REO$_{0.5}$F$_{0.5}$BiCh$_2$-type superconductors [46]. The increase of Se concentration in the BiCh plane results in the enhancement of orbital overlaps between Bi and Ch. It can be considered that the enhanced orbital overlap enhances the carrier mobility, and hence, the metallic conductivity is enhanced. Finally, the calculated PF is shown in Fig. 3(c) as a function of temperature. The PF is clearly enhanced with increasing Se concentration, and large PF values exceeding 4 μW/cmK^2 are observed for $x = 0.8$ and 1 in LaOBiS$_{2-x}$Se$_x$. Indeed, the Se substitution largely enhances the thermoelectric performance in the LaOBiS$_2$ system.

3-3. Densified LaOBiSSe

The experimental results on LaOBiS$_{2-x}$Se$_x$ shown above were based on the polycrystalline pellet samples with a typical relative density of 85-90%. Thus, we densified the LaOBiS$_{2-x}$Se$_x$ samples using a hot-press (HP) instrument under an applied pressure of 50 MPa and annealing temperature of 700 or 800 ℃, with which high density samples were obtained (relative density > 97%) [45,47]. Here, we show the thermoelectric properties of LaOBiSSe because the highest performance was attained in the HP-LaOBiSSe sample among $x = 0$-1.

Due to the uniaxial pressure in the densification process, the obtained sample can possess anisotropic crystal (grain) orientation. So, let us firstly mention the crystal orientation of the HP sample. Figure 4(a) shows the XRD patterns for the powder and pellet samples; for the pellet samples, the scattering vector of X-ray is parallel or perpendicular to the pressing (HP) direction (P$_{//}$ or P$_{\perp}$). The definitions of the P$_{//}$ and P$_{\perp}$ directions are shown in Fig. 4(b). The XRD results propose that the HP process does not affect the phase purity because any impurity phases were not generated.

The peak intensities were different in between $P_{//}$ and $P_{\perp}$, indicating that the obtained sample was oriented as expected. However, we found that the crystal orientation in the HP sample was very weak: the difference of the peak intensities of the ($h00$) and the ($00l$) peaks for $P_{//}$ and $P_{\perp}$ are not large. (If the sample was completely oriented, only the ($h00$) or the ($00l$) peaks should be observed as in the case of thin films.)

Figure 4(c) shows the temperature dependences of ρ for two measurement directions (measured with currents of $I // P_{//}$ or $I // P_{\perp}$). The ρ increases with increasing temperature for both, and the values of ρ for $P_{\perp}$ are clearly lower than those of $P_{//}$, which is consistent to the fact that the ab plane of the LaOBiSSe grains is relatively oriented along the $P_{\perp}$ direction. The BiS_2-based compounds essentially show two-dimensional electrical conduction [48]. Figure 4(d) shows the temperature dependences of S. For both samples, negative S is observed. The absolute values of S for $P_{//}$ are slightly larger than those of $P_{\perp}$, which is also consistent with the difference in the ρ and the crystal orientation. As a result, the PF values for $P_{\perp}$ are larger than those for $P_{//}$.

To estimate ZT, κ was also measured for these samples (Fig. 4(e)). The κ decreases with increasing temperature, and the values of κ for the $P_{\perp}$ direction are clearly larger than those for the $P_{//}$ direction. This result indicates that the thermal conductivity along the c axis is obviously smaller than that along the a axis. Figure 4(f) shows the temperature dependences of ZT for both measurement directions. The values of ZT for $P_{//}$ are slightly larger than those for $P_{\perp}$, and the ZT for these directions at the highest temperature (tested in the study) is almost the same. These results suggest that the thermoelectric performance of LaOBiSSe is not largely affected by the crystal orientation because one direction possesses a good (high) PF, and the other direction possesses a good (low) κ. This characteristic on the insensitivity of ZT to the crystal (grain) orientation may be useful when considering practical application of these $BiCh_2$-based materials.

4. Properties of other layered Bi chalcogenides

Up to here, we focused on the properties of $LaOBiS_2$-based systems. As mentioned with Fig. 1, one of the merits of the Bi-chalcogenide layered compound family is the crystal structure variety. Thus, in this section, we briefly introduce the thermoelectric properties of $REO_{1-x}F_xBiS_2$ (RE = Ce or Nd) and $EuFBiS_2$ with the $REOBiCh_2$-type structure. In addition, the properties of $LaOBiPbS_3$ with the 4-layer-type compound (Fig. 1(d)) at high temperatures are shown.

4-1. $REO_{1-x}F_xBiS_2$

Figures 5(a-c) show the temperature dependences of ρ, S, and PF for $CeO_{1-x}F_xBiS_2$ with x = 0, 0.25, and 0.5. The values of ρ for x = 0 ($CeOBiS_2$) are clearly lower than those of $LaOBiS_2$. It has been reported that the polycrystalline sample of $CeOBiS_2$ shows metallic conductivity at low

temperature [14], which seems to be consistent to the present data. In contrast, the single crystal of CeOBiS$_2$ shows semiconducting behavior at low temperatures [49]. On the basis of these diverse experimental facts in polycrystalline samples and single crystals, the electronic states can be different in between these two sample forms. As a fact, the photoemission experiment suggested that the Ce valence is in the mix-valence state of Ce^{3+} and Ce^{4+} [50], which should provide excess electron carriers to the BiS$_2$ conducting layers. Local structure distortion and/or the effect of the grain size may be affecting the Ce valence and the electronic states of polycrystalline CeOBiS$_2$. The low absolute values of S for CeOBiS$_2$ (Fig. 5(b)) seems to be consistent with the mixed-valence scenario in CeOBiS$_2$ because the absolute value of S of semiconductors generally decreases with increasing carrier concentration. As a result, the PF for CeOBiS$_2$ is lower than that of LaOBiS$_2$ and comparable to electron-doped LaO$_{0.95}$F$_{0.05}$BiS$_2$.

For $x = 0.25$ of CeO$_{1-x}$F$_x$BiS$_2$, the values of ρ are larger than those for $x = 0$. The absolute values of S for $x = 0.25$ are also larger than those of $x = 0$. For $x = 0.5$, the values of ρ and absolute S are lower than those for $x = 0$. These experimental results suggest that the effects of F substitutions to the thermoelectric properties in CeO$_{1-x}$F$_x$BiS$_2$ cannot be simply understood. First, we have to consider the effect of the mixed-valence states of Ce. In addition, we are tuning electron carriers by the F concentration. Furthermore, the carrier mobility should largely affect the electrical transport as shown in LaOBiS$_{2-x}$Se$_x$. Actually, the a-axis is expanded with increasing F concentration in these CeO$_{1-x}$F$_x$BiS$_2$ samples and in the previous reports as well [14]. By simply estimating the in-plane chemical pressure effect in CeO$_{1-x}$F$_x$BiS$_2$, the elongation of the a-axis should result in the decrease in in-plane chemical pressure (decrease in orbital overlap) and carrier mobility. These multiple factors make the understanding of the thermoelectric properties of CeO$_{1-x}$F$_x$BiS$_2$ quite difficult. Anyway, the replacement of the La$_2$O$_2$ blocking layer to the Ce$_2$O$_2$ layer does not positively work in enhancing PF.

Next, let us introduce the properties of NdO$_{1-x}$F$_x$BiS$_2$ with $x = 0.25$ and 0.5; unfortunately, the polycrystalline samples of $x = 0$ cannot be obtained in the system. Figures 5(d-f) show the temperature dependences of ρ, S, and PF for NdO$_{1-x}$F$_x$BiS$_2$. Both samples show similar temperature dependences of ρ and S, but the values of ρ for $x = 0.25$ are lower than those for $x = 0.5$ while the nominal composition of doped F is half in the $x = 0.25$ sample. The almost same values of S would suggest that the effective carrier concentration is almost the same. This assumption is consistent with the fact that the superconducting transition temperature of the NdO$_{1-x}$F$_x$BiS$_2$ system is not sensitive to the F concentration within a wide range of $x = 0.1$-0.7 [16,51,52]. The a-axis of NdO$_{1-x}$F$_x$BiS$_2$ also increases with increasing F concentration. The larger ρ values for $x = 0.5$ than those for $x = 0.25$ may be resulting from the decrease in the in-plane chemical pressure with the a-axis elongation as well as in CeO$_{1-x}$F$_x$BiS$_2$. As facts, the values of PF for NdO$_{1-x}$F$_x$BiS$_2$ are quite low as compared to LaOBiS$_{2-x}$Se$_x$.

As shown here, the replacement of the La_2O_2 blocking layer to the other RE_2O_2 blocking layer does not positively work in enhancing PF. In addition, the Se substitution for the S site cannot be demonstrated in the Ce- or Nd-based compounds. The reason may be due to the ionic radius of Se^{2-}, which would be too large for the Ce_2O_2 or Nd_2O_2 blocking layers. Next, we review the recent studies on $EuFBiS_2$ and $LaOBiPbS_3$.

4-2. $EuFBiS_2$

$EuFBiS_2$ crystalizes in the tetragonal $P4/nmm$ space group, which can be obtained by replacing the La_2O_2 layer of $LaOBiS_2$ to the Eu_2F_2 layer (Fig. 6(c)). This material shows metallic conductivity and shows a superconducting transition at 0.4 K [32]. Goto *et al*. measured thermoelectric properties of $EuFBiS_2$ at high temperatures [53]. Figures 6(a,b) show the temperature dependences of ρ and S for $EuFBiS_2$. At T = 300-623 K, the ρ showed a slight decrease with increasing temperature but the values were almost constant (ρ = 3.5-4 mΩcm). The S at 300 K was -32 μV/K, and the absolute value of S increased with increasing temperature and reached -50 μV/K at 623 K. The estimated κ at 300 K was about 2 W/mK, which was also low and close to that of $LaOBiS_2$. Indeed, low thermal conductivity seems to be a general characteristic of the layered Bi-chalcogenide family. The calculated PF and ZT were 0.71 μW/cmK^2 and 0.02 at 623 K, respectively. We consider that the low ZT (PF) in $EuFBiS_2$ can be attributed to the excess electron carriers as in the case of $CeOBiS_2$. Zhai *et al*. proposed that the Eu valence in $EuFBiS_2$ is not +2 but +2.1-2.3, and the metallic characteristics were resulting from the excess electron carriers doped in the BiS_2 layers due to the mixed-valence state of Eu [32]. The carrier concentration (n) estimated from the Hall measurement is 3.2×10^{21} cm^{-3}, which is clearly larger than those of the parent phases of $REOBiS_2$. Therefore, a high ZT cannot be obtained in $EuFBiS_2$ without compensation of the excess electron carriers in the BiS_2 layers.

4-3. $LaOBiPbS_3$

As introduced in Fig. 1, $LaOBiPbS_3$ has the 4-layer-type conducting layer, which is similar to the Bi_4Te_6 conducting layer of $CsBi_4Te_6$ [3,41]. Hence, this material is very important to discuss how we can enhance the thermoelectric properties of the Bi-chalcogenide layered compound family. Sun *et al*. reported thermoelectric properties of $LaOBiPbS_3$ below the room temperature [41]. The ρ at 300 K was ~8 mΩcm, and the ρ largely increased with decreasing temperature (particularly below 100 K). The S at 300 K was -50 μV/K. The κ at 300 K was ~4 W/mK. Using these data, the PF and ZT at 300 K can be calculated to be 0.31 μW/cmK^2 and 0.0023, respectively.

We examined the thermoelectric properties of $LaOBiPbS_3$ at high temperatures. Figures

7(a-c) show the temperature dependences of ρ, S and PF for LaOBiPbS$_3$. The values of ρ are 7-8 mΩcm at between 300 and 740 K, and the ρ does not show a large change with increasing temperature. In contrast, the absolute values of S shows a large increase with increasing temperature. The S at 740 K is -92 μV/K. Hence, the calculated PF largely increases with increasing temperature and reaches 1 μW/cmK^2 at 740 K. Although the values of PF for LaOBiPbS$_3$ are still lower than those for LaOBiSSe, the PF will be enhanced by increasing carrier mobility as demonstrated in LaOBiS$_{2-x}$Se$_x$.

5. Summary and possible strategies for a high thermoelectric performance

We reviewed the crystal structure variation and the physical properties of the new Bi-chalcogenide layered compound family. Here, we briefly summarize the evolution of thermoelectric properties by the element substitution or the manipulation of the layered structure and would like to discuss the possible strategies for a high thermoelectric performance in the layered Bi-chalcogenide compound family. One of the advantages of the layered Bi-chalcogenide compounds as a thermoelectric material is the low thermal conductivity. The values of κ are quite lower than that of the other chalcogenides or other inorganic materials with electrical conduction. In addition, as shown in the part of LaOBiSSe, the κ decreases with introducing disorder as the Se substitution for the S site in LaOBiS$_{2-x}$Se$_x$. Therefore, the thermal conductivity will be tunable at the final stage of the material design of Bi-chalcogenide thermoelectric materials. Thus, we need to enhance PF at the early stage, and now, we are exploring new materials with PF higher than that of LaOBiSSe. On the basis of the results of the electron doping in LaO$_{1-x}$F$_x$BiS$_2$, the excess electron carriers should degrade the PF. In addition, the compounds containing self-doped carriers, such as CeOBiS$_2$ or EuFBiS$_2$, shows a lower performance due to the excess carriers as well. Namely, the parent compound with a band gap should be preferable for a high PF material, which seems to be consistent with the Mott relationship (S can be expressed as a function of T/n) as used in the study of LaO$_{1-x}$F$_x$BiS$_2$ [13]. Therefore, the lower n would result in a high absolute value of S in this system. To discuss this assumption, we plotted the n and the S reported in Refs. 13, 32, 41, 45, and 53 in Fig. 8. The values of n for these compounds were estimated from the Hall measurements by assuming the single-band model for contributing carriers, which are electrons in the present system. Since the Hall coefficient of the electron-doped compounds could not be explained from the single-band model [13], we excluded those electron-doped compounds from this plot. At least, the data points in Fig. 8 ride on a single slope: the absolute values of S are related to the n. Thus, a lower n should be needed for a larger value of absolute S. Next, we need to decrease the ρ without decrease of absolute S. The strategy to achieve this situation should be the enhancement of in-plane chemical pressure effect, which can increase the carrier mobility by the enhancement of in-plane orbital overlaps. On the basis

10

of this scenario, the Bi^{3+}-Se^{2-} or the Bi^{3+}-Te^{2-} bonding will be preferable than the Bi^{3+}-S^{2-} bonding. In addition, the Pb^{2+} ion will be useful to enhance the in-plane chemical pressure because the Pb^{2+} possesses a large ionic radius. Furthermore, the crystal structure symmetry lowering from tetragonal to monoclinic (or orthorhombic) may be useful to enhance the carrier mobility. The $LaOBiCh_2$ structure can be distorted from tetragonal (*P4/nmm*) to monoclinic (*P2$_1$/m*). In the monoclinic structure, Bi-Ch zigzag chains form in the conducting plane, which should strongly affect the electronic states [42,54,55]. With these possible strategies for enhancing *PF* in the layered Bi-chalcogenide compounds, we are going to explore a breakthrough material for the achievement of the novel thermoelectric applications.

References

[1] Shakouri, A., Recent Developments in Semiconductor Thermoelectric Physics and Materials. (2011). Annu. Rev. Mater. Res. 41, 399-431.

[2] Nolas, G. S., Sharp, J. W. & Goldsmid, H. J. (2001). Thermoelectrics: Basic Principles and New Materials Developments. Berlin/Heidelberg: Springer.

[3] Chung, D. Y., Hogan, T., Brazis, P., Rocci-Lane, M., Kannewurf, C., Bastea, M., Uher, C. & Kanatzidis, M. G. (2000). $CsBi_4Te_6$: A High-Performance Thermoelectric Material for Low-Temperature Applications. Science 287, 1024-1027.

[4] Hicks, L. D. & Dresselhaus, M. S. (1993). Effect of quantum-well structures on the thermoelectric figure of merit. Phys. Rev. B 47, 12727-12731.

[5] Venkatasubramanian, R., Siivola, E., Colpitts, T. & O'Quinn, B. (2001). Thin-film thermoelectric devices with high room-temperature figures of merit. Nature 413, 597-602.

[6] Takahata, K., Iguchi, Y., Tanaka, D., Itoh, T. & Terasaki, I. (2000). Low thermal conductivity of the layered oxide $(Na,Ca)Co_2O_4$: Another example of a phonon glass and an electron crystal. Phys. Rev. B 61, 12551-12555.

[7] Funahashi, R., Matsubara, I., Ikuta, H., Takeuchi, T., Mizutani, U. & Sodeoka, S. (2000). An oxide single crystal with high thermoelectric performance in air. Jpn. J. Appl. Phys. 39, L1127-L1129.

[8] Shikano, M. & Funahashi, R. (2003). Electrical and thermal properties of single-crystalline $(Ca_2CoO_3)_{0.7}CoO_2$ with a $Ca_3Co_4O_9$ structure. Appl. Phys. Lett. 82, 1851-1853.

[9] Mizuguchi, Y., Fujihisa, H., Gotoh, Y., Suzuki, K., Usui, H., Kuroki, K., Demura, S., Takano, Y., Izawa, H. & Miura, O. (2012). BiS_2-based layered superconductor $Bi_4O_4S_3$. Phys. Rev. B 86, 220510(1-5).

[10] Mizuguchi, Y., Demura, S., Deguchi, K., Takano, Y., Fujihisa, H., Gotoh, Y., Izawa, H. & Miura, O. (2012). Superconductivity in novel BiS_2-based layered superconductor $LaO_{1-x}F_xBiS_2$. J. Phys. Soc. Jpn. 81, 114725(1-5).

[11] Mizuguchi, Y. (2015). Review of superconductivity in BiS_2-based layered materials. J. Phys. Chem. Solids 84, 34–48.

[12] Usui, H., Suzuki, K. & Kuroki, K. (2012). Minimal electronic models for superconducting BiS_2 layers. Phys. Rev. B 86, 220501(1-5).

[13] Pallecchi, I., Lamura, G., Putti, M., Kajitani, J., Mizuguchi, Y., Miura, O., Demura, S., Deguchi, K & Takano, Y. (2014). Effect of high-pressure annealing on the normal-state transport of $LaO_{0.5}F_{0.5}BiS_2$. Phys. Rev. B 89, 214513 (1-6).

[14] Xing, J., Li, S., Ding, X., Yang, H. & Wen, H. H. (2012). Superconductivity Appears in the Vicinity of an Insulating-Like Behavior in $CeO_{1-x}F_xBiS_2$. Phys. Rev. B 86, 214518(1-5).

[15] Jha, R., Kumar, A., Singh, S. K. & Awana, V. P. S. (2013). Synthesis and superconductivity of

new BiS_2 based superconductor $PrO_{0.5}F_{0.5}BiS_2$. J. Supercond. Nov. Magn. 26, 499-502.

[16] Demura, S., Mizuguchi, Y., Deguchi, K., Okazaki, H., Hara, H., Watanabe, T., Denholme, S. J., Fujioka, M., Ozaki, T., Fujihisa, H., Gotoh, Y., Miura, O., Yamaguchi, T., Takeya, H. & Takano, Y. (2013). BiS_2-based superconductivity in F-substituted $NdOBiS_2$. J. Phys. Soc. Jpn. 82, 033708(1-3).

[17] Thakur, G. S., Selvan, G. K., Haque, Z., Gupta, L. C., Samal, S. L., Arumugam, S & Ganguli, A. K. (2015). Synthesis and properties of $SmO_{0.5}F_{0.5}BiS_2$ and enhancement in Tc in $La_{1-y}Sm_yO_{0.5}F_{0.5}BiS_2$. Inorg. Chem. 54, 1076-1081.

[18] Yazici, D., Huang, K., White, B. D., Chang, A. H., Friedman, A. J. & Maple, M. B. (2012). Superconductivity of F-substituted $LnOBiS_2$ (Ln=La, Ce, Pr, Nd, Yb) compounds. Philos. Mag. 93, 673-680.

[19] Shao, J., Yao, X., Liu, Z., Pi, L., Tan, S., Zhang, C. & Zhang, Y. (2015). Superconductivity in $BiO_{1-x}F_xBiS_2$ and possible parent phase of $Bi_4O_4S_3$ superconductor. Supercond. Sci. Technol. 28, 015008(1-6).

[20] Okada, T., Ogino, H., Shimoyama, J.-I. & Kishio, K. (2015). Topotactic synthesis of a new BiS_2-based superconductor $Bi_2(O,F)S_2$. Appl. Phys. Express, 8, 023102(1-4).

[21] Miura, A., Mizuguchi, Y., Takei, T., Kumada, N., Magome, E., Moriyoshi, C., Kuroiwa, Y. & Tadanaga, K. (2016). Structures and Optical Properties of Bi_2OS_2 and $LaOBiS_2$. Solid State Commun. 227, 19-22.

[22] Nagao, M. Growth and characterization of $R(O,F)BiS_2$ (R = La, Ce, Pr, Nd) superconducting single crystals. Nov. Supercond. Mater. arXiv:1511.00219 (in printing).

[23] Jeon, I., Yazici, D., White, B. D., Friedman, A. J. & Maple, M. B. (2014). Effect of yttrium substitution on the superconducting properties of $La_{1-x}Y_xO_{0.5}F_{0.5}BiS_2$. Phys. Rev. B 90, 054510(1-7).

[24] Yazici, D., Huang, K., White, B. D., Jeon, I., Burnett, V. W., Friedman, A. J., Lum, I. K., Nallaiyan, M., Spagna, S. & Maple, M. B. (2013). Superconductivity induced by electron doping in the system $La_{1-x}M_xOBiS_2$ (M = Ti, Zr, Hf, Th). Phys. Rev. B 87, 174512(1-8).

[25] Wang, X. C., Chen, D. Y., Guo, Q., Yu, J., Ruan, B. B., Mu, Q. G., Chen, G. F. & Ren, Z. A. Enhanced superconductivity in F-doped $LaO_{1-x}F_xBiSSe$. arXiv:1404.7562.

[26] Hiroi, T., Kajitani, J., Omachi, A., Miura, O. & Mizuguchi, Y. (2015). Evolution of Superconductivity in BiS_2-Based Superconductor $LaO_{0.5}F_{0.5}Bi(S_{1-x}Se_x)_2$. J. Phys. Soc. Jpn. 84, 024723(1-4).

[27] Tanaka, M., Yamaki, T., Matsushita, Y., Fujioka, M., Denholme, S. J., Yamaguchi, T., Takeya, H. & Takano, Y. (2015). Site Selectivity on Chalcogen Atoms in Superconducting $La(O,F)BiSSe$. Appl. Phys. Lett. 106, 112601(1-5).

[28] Mizuguchi, Y., Hiroi, T. & Miura, O. Superconductivity phase diagram of Se-substituted $CeO_{0.5}F_{0.5}Bi(S_{1-x}Se_x)_2$. arXiv:1511.03787. J. Phys.: Conf. Ser. (in printing).

[29] Hiroi, T., Kajitani, J., Omachi, A., Miura, O. & Mizuguchi, Y. (2015). Element Substitution

Effect on Superconductivity in BiS$_2$-Based NdO$_{1-x}$F$_x$BiS$_2$. J. Supercond. Nov. Magn. 28, 1149-1153.

[30] Maziopa, A. K., Guguchia, Z., Pomjakushina, E., Pomjakushin, V., Khasanov, R., Luetkens, H., Biswas, P., Amato, A., Keller, H. & Conder, K. (2014). Superconductivity in a new layered bismuth oxyselenide: LaO$_{0.5}$F$_{0.5}$BiSe$_2$. J. Phys.: Condens. Matter 26, 215702(1-5).

[31] Lei, H., Wang, K., Abeykoon, M., Bozin, E. S. & Petrovic, C. (2013). New layered oxysulfide SrFBiS$_2$. Inorg. Chem. 52, 10685-10689.

[32] Zhai, H. F., Tang, Z. T., Jiang, H., Xu, K., Zhang, K., Zhang, P., Bao, J. K., Sun, Y. L., Jiao, W. H., Nowik, I., Felner, I., Li, Y. K., Xu, X. F., Tao, Q., Feng, C. M., Xu, Z. A. & Cao, G. H. (2014). Possible Charge-density wave, superconductivity and f-electron valence instability in EuBiS$_2$F. Phys. Rev. B 90, 064518(1-9).

[33] Lin, X., Ni, X., Chen, B., Xu, X., Yang, X., Dai, J., Li, Y., Yang, X., Luo, Y., Tao, Q., Cao, G. & Xu, Z. (2013). Superconductivity induced by La doping in Sr$_{1-x}$La$_x$FBiS$_2$. Phys. Rev. B 87, 020504(1-4).

[34] Jha, R., Tiwari, B. & Awana, V. P. S. (2015). Appearance of bulk Superconductivity under Hydrostatic Pressure in Sr$_{0.5}$RE$_{0.5}$FBiS$_2$ (RE = Ce, Nd, Pr and Sm) new compounds. J. Appl. Phys. 117, 013901(1-7).

[35] Zhai, H. F., Zhang, P., Tang, Z. T., Bao, J. K., Jiang, H., Feng, C. M., Xu, Z. A. & Cao, G. H.. Coexistence of superconductivity and complex 4f magnetism in Eu$_{0.5}$Ce$_{0.5}$BiS$_2$F. arXiv:1505.06447.

[36] Zhai, H. F., Zhang, P., Wu, S. Q., He, C. Y., Tang, Z. T., Jiang, H., Sun, Y. L., Bao, J. K., Nowik, I., Felner, I., Zeng, Y. W., Li, Y. K., Xu, X. F., Tao, Q., Xu, Z. A. & Cao, G. H. (2014). Anomalous Eu Valence State and Superconductivity in Undoped Eu$_3$Bi$_2$S$_4$F$_4$. J. Am. Chem. Soc. 136, 15386-15393.

[37] Zhang, P., Zhai, H. F., Tang, Z. J., Li, L., Li, Y. K., Chen, Q., Chen, J., Wang, Z., Feng, C. M., Cao, G. H. & Xu, Z. A. (2015). Superconductivity enhanced by Se doping in Eu$_3$Bi$_2$(S,Se)$_4$F$_4$. EPL 111, 27002(p1-p6).

[38] Miura, A., Mizuguchi, Y., Sugawara, T., Wang, Y., Takei, T., Kumada, N., Magome, E., Moriyoshi, C., Kuroiwa, Y., Miura, O. & Tadanaga, K. (2015). Structural Difference in Superconductive and Nonsuperconductive Bi–S Planes within Bi$_4$O$_4$Bi$_2$S$_4$ Blocks. Inorg. Chem. 54, 10462-10467.

[39] Phelan, W. A., Wallace, D. C., Arpino, K. E., Neilson, J. R., Livi, K. J., Seabourne, C. R., Scott, A. J. & McQueen, T. M. (2013). Stacking Variants and Superconductivity in the Bi-O-S System. J. Am. Chem. Soc. 135, 5372-5374.

[40] Li, L., Parker, D., Babkevich, P., Yang, L., Ronnow, H. M. & Sefat, A. S. (2015). Superconductivity in Semimetallic Bi$_3$O$_2$S$_3$. Phys. Rev. B 91, 104511(1-5).

[41] Sun, Y. L., Ablimit, A., Zhai, H. F., Bao, J. K., Tang, Z. T., Wang, X. B., Wang, N. L., Feng, C. M. & Cao, G. H. (2014). Design and Synthesis of a New Layered Thermoelectric Material

LaPbBiS$_3$O. Inorg. Chem. 53, 11125-11129.

[42] Sagayama, R., Sagayama, H., Kumai, R., Murakami, Y., Asano, T., Kajitani, J., Higashinaka, R., Matsuda, T. D. & Aoki, Y. (2015). Symmetry Lowering in LaOBiS$_2$: A Mother Material for BiS$_2$-Based Layered Superconductors. J. Phys. Soc. Jpn. 84, 123703(1-5).

[43] Omachi, A., Kajitani, J., Hiroi, T., Miura, O. & Mizuguchi, Y. (2014). High-temperature thermoelectric properties of novel layered bismuth-sulfide LaO$_{1-x}$F$_x$BiS$_2$. J. Appl. Phys. 115, 083909(1-3).

[44] Mizuguchi, Y., Omachi, A., Goto, Y., Kamihara, Y., Matoba, M., Hiroi, T., Kajitani, J. & Miura, O. (2014). Enhancement of thermoelectric properties by Se substitution in layered bismuth-chalcogenide LaOBiS$_{2-x}$Se$_x$. J. Appl. Phys. 116, 163915(1-4).

[45] Nishida, A., Nishiate, H., Lee, C. H., Miura, O. & Mizuguchi, Y. (2015). Electronic Origins of Large Thermoelectric Power Factor of LaOBiS$_{2-x}$Se$_x$. arXiv:1511.09133.

[46] Mizuguchi, Y., Miura, A., Kajitani, J., Hiroi, T., Miura, O., Tadanaga, K., Kumada, N., Magome, E., Moriyoshi, C. & Kuroiwa, Y. (2015). In-plane chemical pressure essential for superconductivity in BiCh$_2$-based (Ch: S, Se) layered structure. Sci. Rep. 5, 14968(1-8).

[47] Nishida, A., Miura, O., Lee, C. H. & Mizuguchi, Y. (2015). High thermoelectric performance and low thermal conductivity of densified LaOBiSSe. Appl. Phys. Express 8, 111801.

[48] Nagao, M., Miura, A., Watauchi, S., Takano, Y. & Tanaka, I. (2015). C-axis electrical resistivity of PrO$_{1-a}$F$_a$BiS$_2$ single crystals. Jpn. J. Appl. Phys. 54, 083101(1-5).

[49] Higashinaka, R., Asano, T., Nakashima, T., Fushiya, K., Mizuguchi, Y., Miura, O., Matsuda, T. D. & Aoki, Y. (2015). Pronounced-Log T Divergence in Specific Heat of Nonmetallic CeOBiS$_2$: A Mother Phase of BiS$_2$-Based Superconductor. J. Phys. Soc. Jpn. 84, 023702(1-4).

[50] Sugimoto T., Joseph, B., Paris, E., Iadecola, A., Mizokawa, T., Demura, S., Mizuguchi, Y., Takano, Y. & Saini, N. L. (2014). Role of the Ce valence in the coexistence of superconductivity and ferromagnetism of CeO$_{1-x}$F$_x$BiS$_2$ revealed by Ce L$_3$-edge x-ray absorption spectroscopy. Phys. Rev. B 89, 201117(1-5).

[51] Jha, R. & Awana, V. P. S. (2014). Superconducting properties of BiS$_2$ based superconductor NdO$_{1-x}$F$_x$BiS$_2$ (x = 0 to 0.9). Mat. Res. Exp. 1, 016002(1-10).

[52] Omachi, A., Hiroi, T., Kajitani, J., Miura, O. & Mizuguchi, Y. (2014). Importance of uniaxial compression for the appearance of superconductivity in NdO$_{1-x}$F$_x$BiS$_2$. J. Phys.: Conf. Ser., 507, 012033(1-4).

[53] Goto, Y., Kajitani, J., Mizuguchi, Y., Kamihara, Y. & Matoba, M. (2015). Electrical and Thermal Transport of Layered Bismuth-chalcogenide EuBiS$_2$F at temperatures between 300 and 623 K. J. Phys. Soc. Jpn. 84, 085003(1-2).

[54] Tomita, T., Ebata, M., Soeda, H., Takahashi, H., Fujihisa, H., Gotoh, Y., Mizuguchi, Y., Izawa, H., Miura, O., Demura, S., Deguchi, K. & Takano, Y. (2014). Pressure-induced Enhancement of

Superconductivity in BiS_2-layered $LaO_{1-x}F_xBiS_2$. J. Phys. Soc. Jpn. 83, 063704(1-4).

[55] Ochi, M., Akashi, R. & Kuroki, K. Strong bilayer coupling induced by the symmetry breaking in the monoclinic phase of BiS_2-based superconductors. arXiv:1512.03884.

[56] Momma, K. & Izumi, F. (2008). VESTA: a three-dimensional visualization system for electronic and structural analysis. J. Appl. Crystallogr. 41, 653-658.
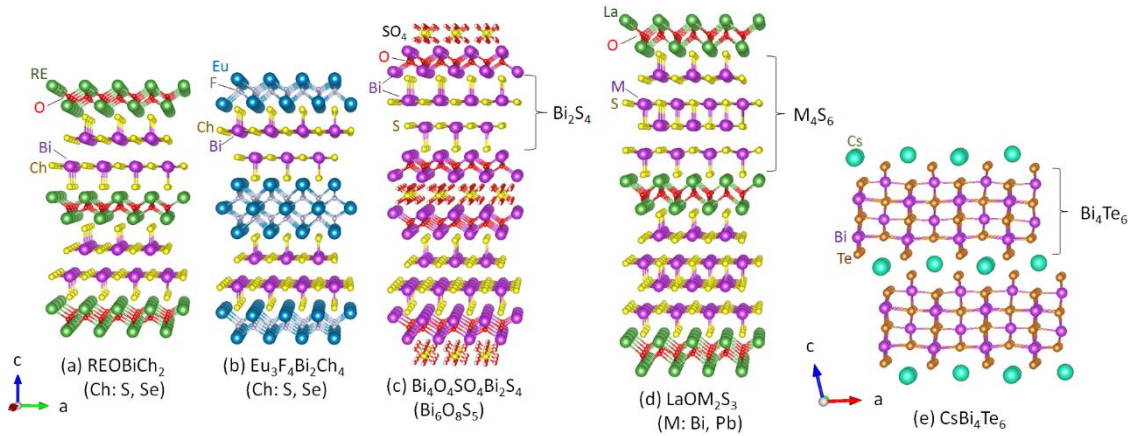
Fig. 1. Schematic images of the crystal structure of various Bi-chalcogenide compounds. (a-c) Typical BiS_2-based compounds: (a) $REOBiCh_2$ (RE: rare earth or Bi; Ch: S, Se) [10,30], (b) $Eu_3F_4Bi_2Ch_4$ [36,37], and (c) $Bi_4O_4SO_4Bi_2S_4$ [9]. The electrically conducting layer of these compounds is the two-layer-type Bi_2S_4 layer. (d) $LaOM_2S_3$ (M: Bi, Pb) [41]. The M_4S_6 conducting layer of $LaOM_2S_3$ is similar to the Bi_4Te_6 layer of (e) $CsBi_4Te_6$ [3]. The crystal structure images were prepared using VESTA software [56]
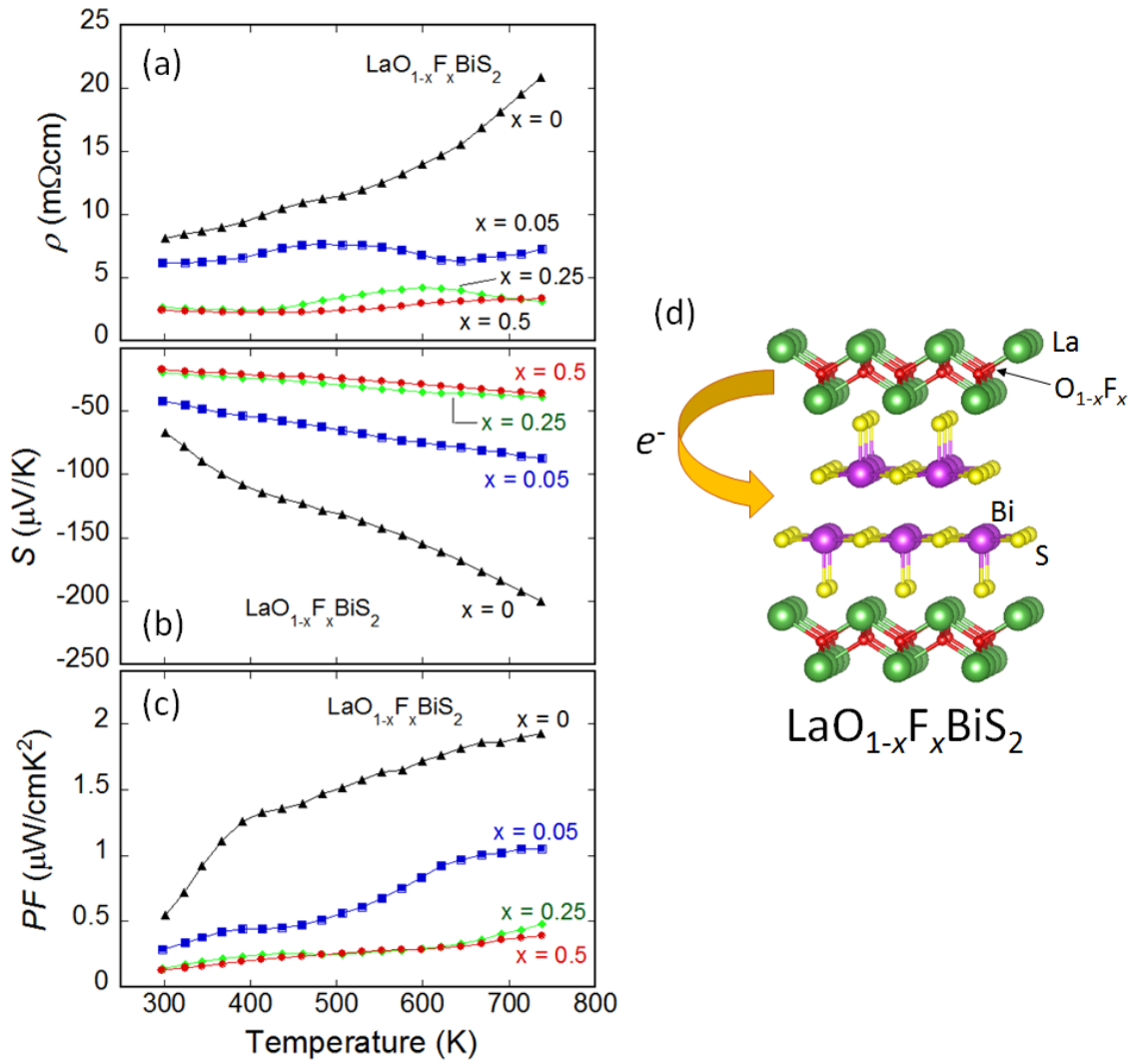
Fig. 2. (a-c) Temperature dependences of (a) electrical resistivity (ρ) (b) Seebeck coefficient (S), and (c) power factor (PF) for LaO$_{1-x}$F$_x$BiS$_2$. (d) Schematic image of the crystal structure of LaO$_{1-x}$F$_x$BiS$_2$ and electron doping scenario. Refer to Ref. 43 (J. Appl. Phys. 115, 083909 (2014)) for original data.
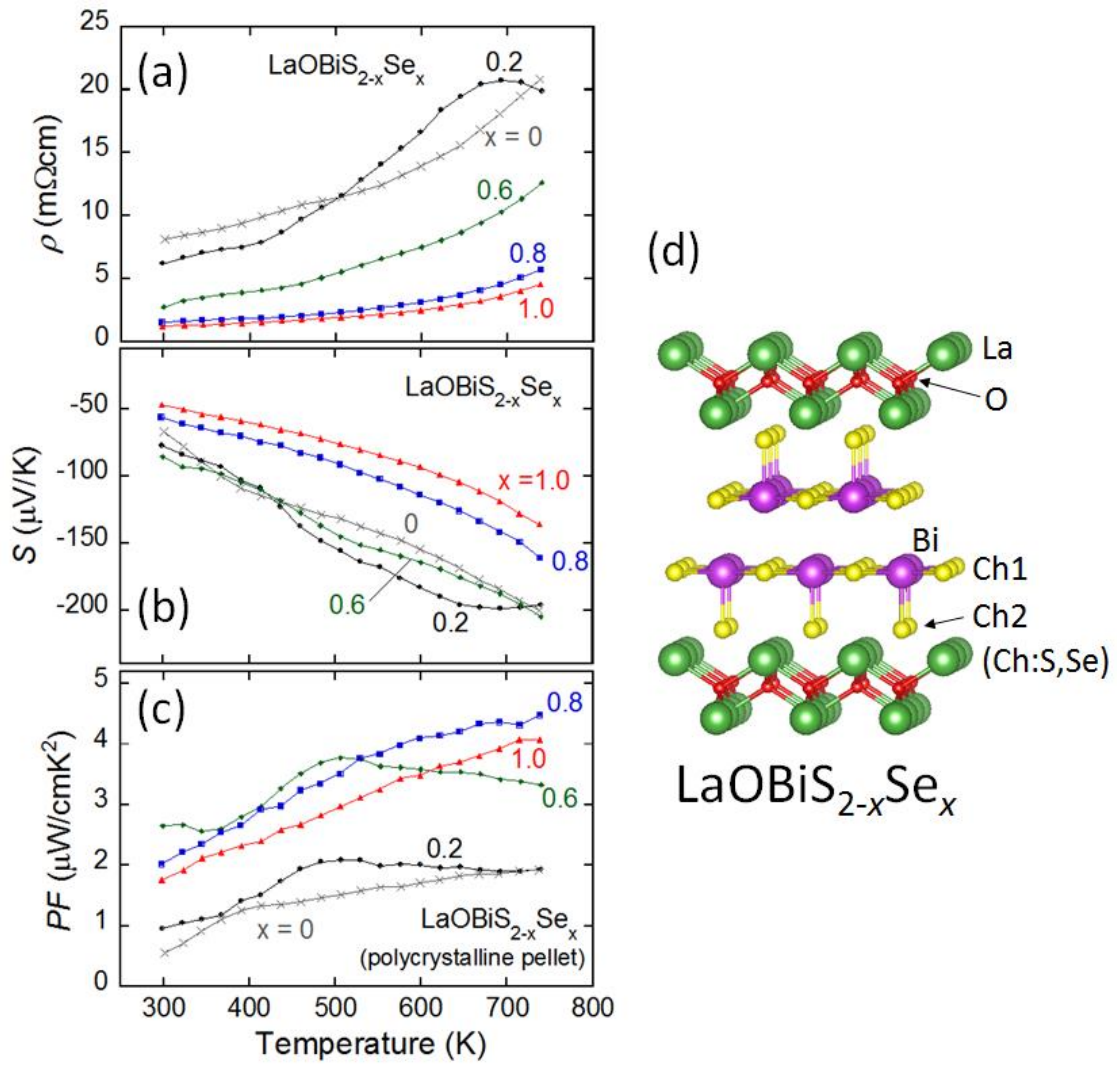
Fig. 3. (a-c) Temperature dependences of (a) electrical resistivity (ρ) (b) Seebeck coefficient (S), and (c) power factor (PF) for LaOBiS$_{2-x}$Se$_x$. (d) Schematic image of the crystal structure of LaOBiS$_{2-x}$Se$_x$ and the definitions of the Ch1 and Ch2 sites. Refer to Ref. 44 (J. Appl. Phys. 116, 163915 (2014)) for original data.
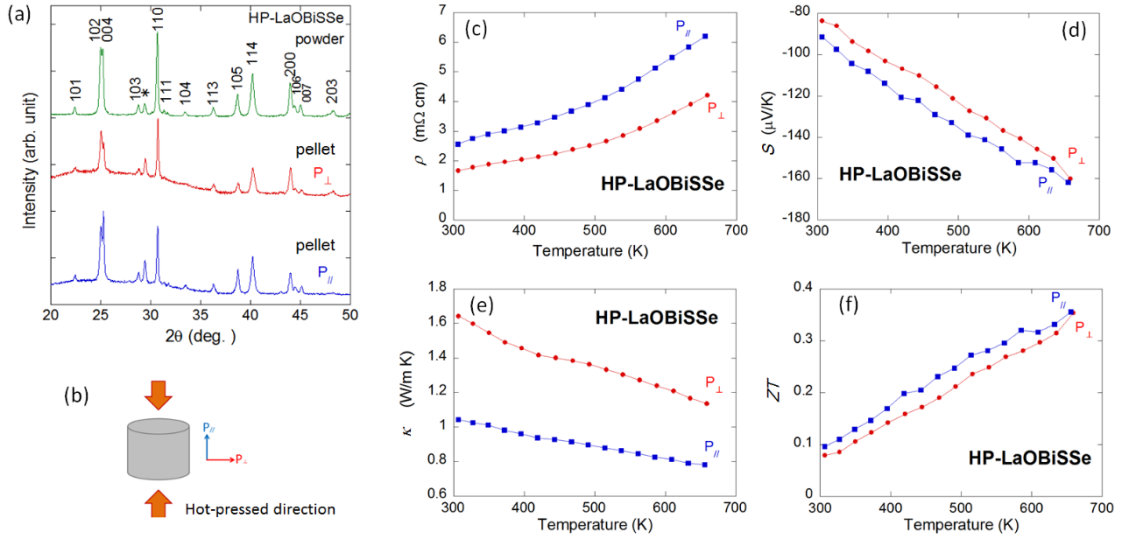
Fig. 4. (a) XRD patterns for hot-pressed (HP) LaOBiSSe ($x = 1$). The Miller indices are shown with the top profile. The asterisk indicates the impurity (La$_2$O$_3$: 7% against the major phase) peak. To investigate the crystal structure anisotropy, XRD measurements were performed for polished pellets with two scattering vectors of P$_{//}$ and P$_\perp$. (b) Schematic image for the definitions of the measurement directions of P$_{//}$ and P$_\perp$ and the hot-pressing direction. (c-f) Temperature dependences of (c) electrical resistivity (ρ), (d) Seebeck coefficient (S), (e) thermal conductivity (κ), and dimensionless figure-of-merit (ZT) for HP-LaOBiSSe. Refer to Ref. 47 (Appl. Phys. Express 8, 111801 (2015)) for original data.
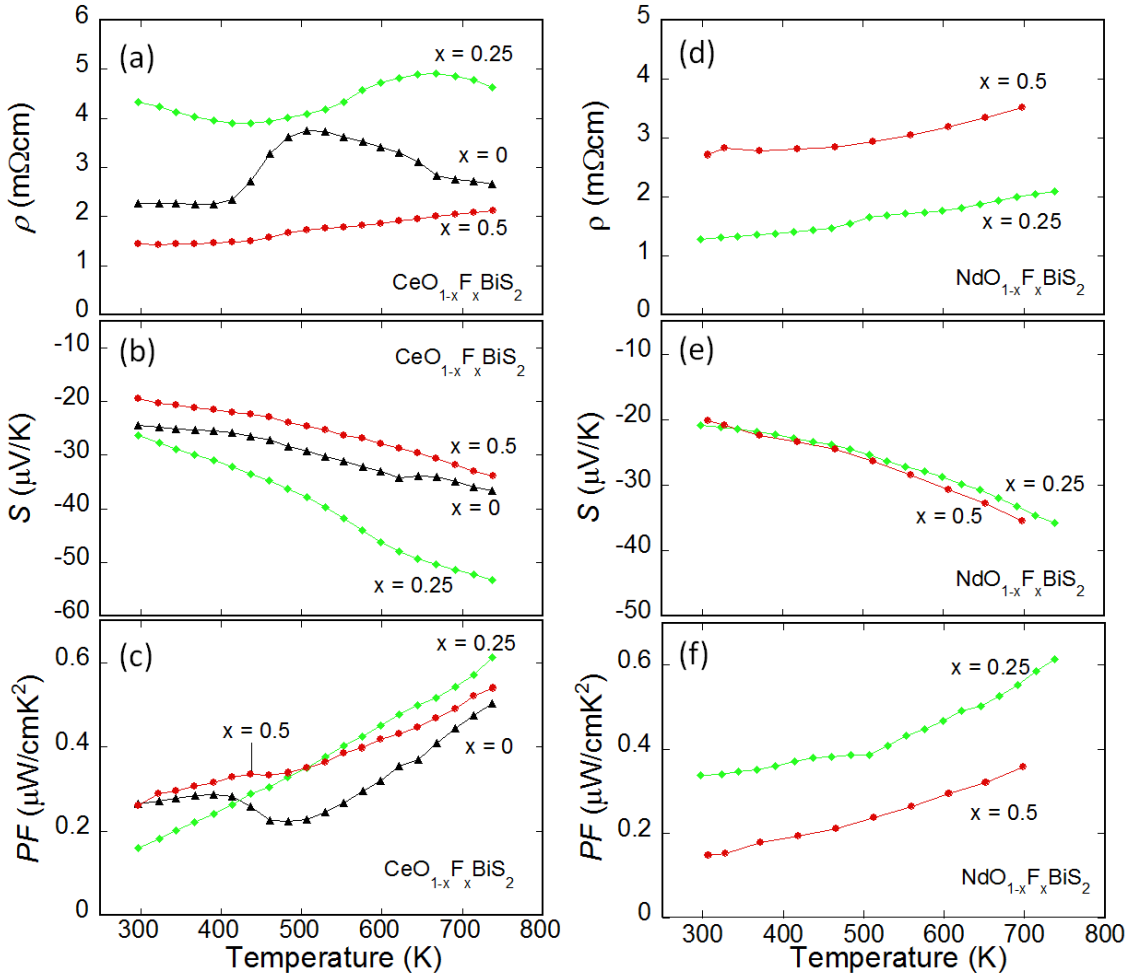
Fig. 5. (a-c) Temperature dependences of (a) electrical resistivity (ρ), Seebeck coefficient (S), and power factor (PF) for $CeO_{1-x}F_xBiS_2$. (d-f) Temperature dependences of (d) ρ, (e) S, and (f) PF for $NdO_{1-x}F_xBiS_2$. Note that $NdOBiS_2$ ($x = 0$) was not obtained with the solid-state-reaction synthesis.
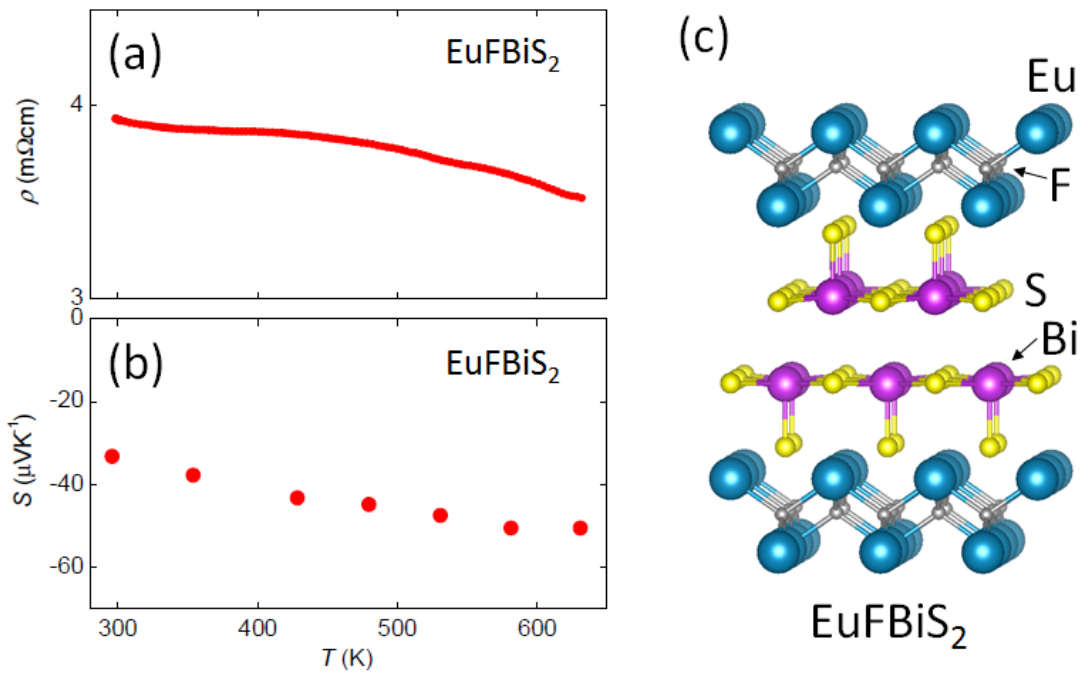
Fig. 6. Temperature dependences of (a) electrical resistivity (ρ) and (b) Seebeck coefficient (S) for EuFBiS$_2$. (c) Schematic image of the crystal structure of EuFBiS$_2$. Refer to Ref. 53 (J. Phys. Soc. Jpn. 84, 085003 (2015)) for the original data for Figs. 6(a,b).
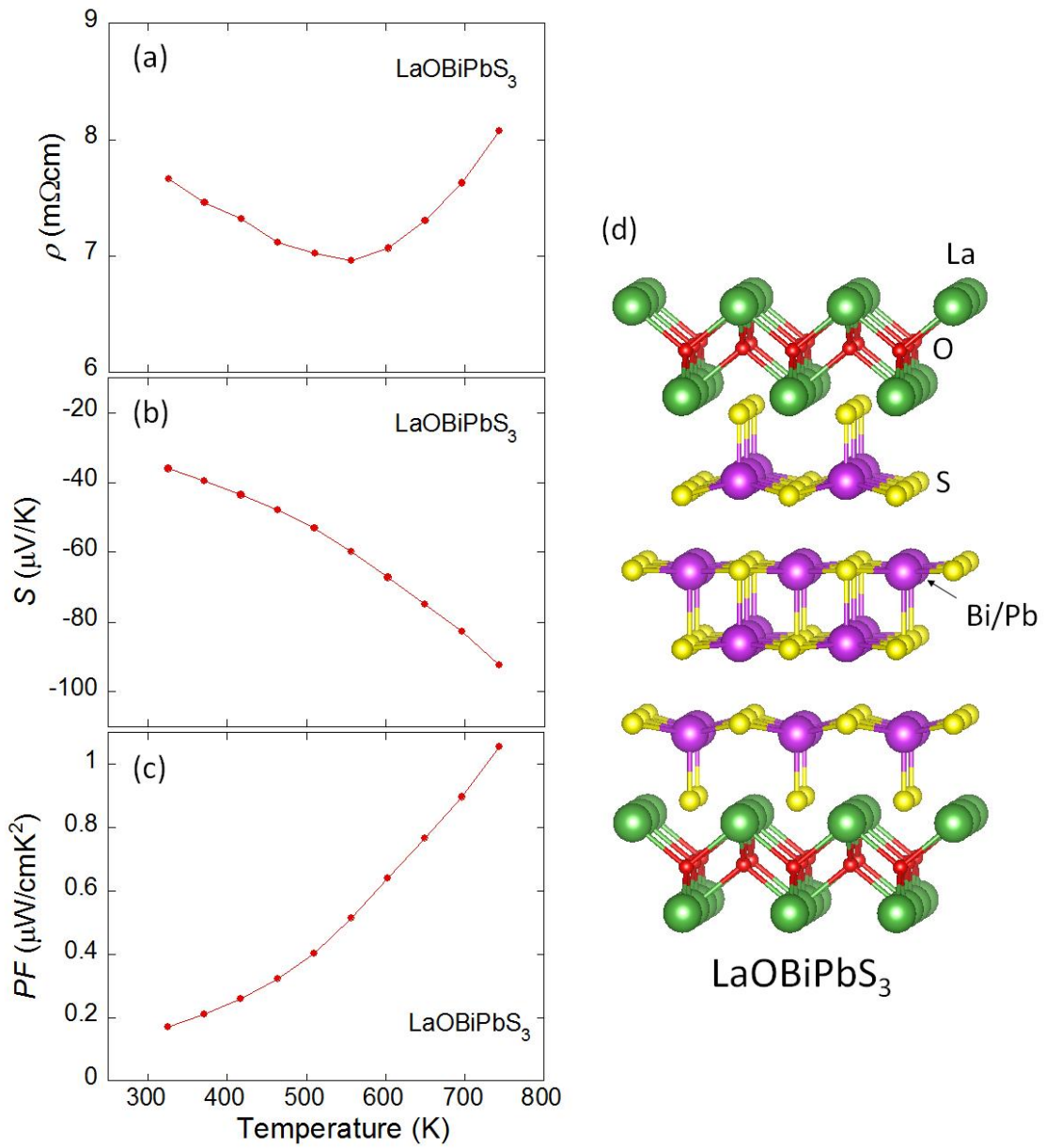
Fig. 7. (a-c) Temperature dependences of (a) electrical resistivity (ρ), Seebeck coefficient (S), and power factor (PF) for LaOBiPbS$_3$. (d) Schematic image of the crystal structure of LaOBiPbS$_3$.
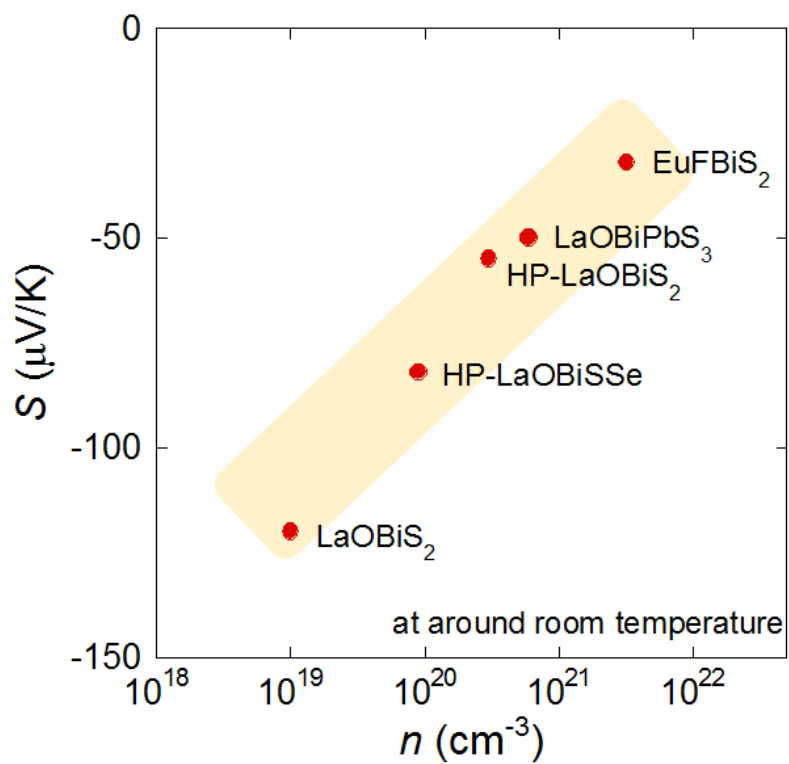
Fig. 8. The Seebeck coefficient (S) for several Bi-chalcogenide samples (parent phases) are plotted as a function of the carrier concentration (n) (log scale for n).